

Laboratory test on crack development in mudstone under the action of dry-wet cycles

Ming Hu¹ · Yuanxue Liu¹ · Jianbo Ren¹ · Runze Wu¹ · Yu Zhang¹

Received: 13 November 2016 / Accepted: 23 May 2017 / Published online: 20 June 2017
© Springer-Verlag Berlin Heidelberg 2017

Abstract Rock masses in southwest China are dominated by alternating layers of sandstone and mudstone. When exposed to natural conditions, mudstone is vulnerable to disintegration, causing the overlying sandstone to be extremely likely to collapse under the action of a load or other conditions. An effective and innovative experimental method to characterize weathering processes would contribute to collapse prevention. In this study, a customized test unit, including a model test container, a lever-loading device and a thermostat-controlled heating plate, was applied to explore the mechanism of crack development in mudstone over multiple dry-wet cycles. The crack width, vertical displacement and wetted area were measured to analyse the slaking mechanism acting during these cycles. The results show that tiny cracks appeared on the surface of the sample after heating and that the vertical displacement increased in the upward direction because of swelling of mudstone. The crack width expanded with increasing water exposure, but after the water infiltrated the surface of the sample, the crack width decreased. The external surface of the sample was gradually infiltrated in the second dry-wet cycle, and the infiltration area increased continually. The infiltrating speed grew progressively faster with each cycle, and the number and size of internal cracks monotonically increased. The sample fractured as a result of crack extension. These results have theoretical significance regarding the ground collapse of alternating layers of sandstone and mudstone.

Keywords Mudstone · Crack development · Dry-wet cycles · Temperature-induced stress · Fluid effects

Introduction

Alternating layers of sandstone and mudstone are widely distributed in southwest China and generally exhibit favourable stability. However, the number of surface collapse incidents has increased in recent years. The surface collapse mechanism of this geological condition is different from that of karst collapse, mining collapse and loess hydrocompaction. There is theoretical and practical significance to studying the collapse mechanism of this geological condition for preventing and responding to disasters. Mudstone weathers and disintegrates easily after multiple dry-wet cycles, which provides the conditions to generate a cave inside the rock mass. This configuration is more likely to collapse under the action of an overlying load. Thus, studying the weathering process of mudstone under dry-wet cycles through experimentation can provide an experimental and theoretical basis for surface collapse of alternating layers of sandstone and mudstone.

Mudstone is a type of soft rock that is formed through the long-term compaction of silt and clay; it exhibits low permeability (Lee et al. 2013). Many phenomena and engineering problems are associated with mudstone (Al-homoud et al. 1996; Imumorin and Azam 2011). Micro cracks and flaws exist in the compaction period of mudstone; thus, when it is exposed to air, it shrinks and cracks due to water loss and differential stresses. Differential stresses are created as mudstone containing expanding clay minerals adsorbs water, and the interaction between the entrapped air and expanding materials results in the deterioration of mudstone (Seedsman 1993; Molinda et al. 2006). Thus, the action of water on mudstone can degrade its mechanical strength (Ojo and Brook

✉ Yuanxue Liu
lyuanxue@vip.sina.com

¹ Chongqing Key Laboratory of Geomechanics and Geoenvironment Protection, People's Liberation Army Logistical Engineering University, Chongqing 401311, China

1990; Yoshida et al. 1997; Lashkaripour 2002; Poulsen et al. 2014; Lu et al. 2016), cause swelling in its composite clay minerals (Einstein 1996; Zhang et al. 2016; Zhang et al. 2017), and promote crack propagation through the rock mass (Pejon and Zuquette 2002; Arnould 2006; Guo et al. 2012; Gautam and Shakoor 2013; Lu et al. 2016).

Many researchers have noted that the mechanisms of the water-weakening effect are multifaceted. The water-weakening effect is greater in clay-rich rocks than in quartz-rich rocks (Goodman 1989; Poulsen et al. 2014). Clay-rich rocks can swell and significantly soften after absorbing water, which degrades their mechanical strength (Erguler and Ulusay 2009). Gamble (1971), Phienweij (1987) determined that disintegration arises mainly by water absorption and changes in the water content. The average decay rate of purple mudstones increased with increasing rock moisture content (Zhang et al. 2016). Eeckhout (1976) and Silva et al. (2008) suggested that the mechanisms of the water-weakening effect include decreasing surface fracture energy, increasing pore pressure, decreasing capillary tension, stress corrosion, decreasing friction and chemical degradation. Lashkaripour and Boomeri (2002) noted that the mineralogical composition and texture of the rocks were factors in the slake durability of weak rocks. Jiang et al. (2014) applied computerized tomographic scanning to the study of water-induced weakening of mudstone and provided visual evidence for the assessment of mudstone performance with respect to the stability of landslides, debris flows and susceptibility of subsidence in mudstone strata. Ashby et al. (1970) established a low-stress mode for rock grain boundary sliding with diffusion material migration; the dissolution and formation of minerals in the chemical reaction between water and rock, as described by this model, follow the mechanical properties of soft rocks during softening. All these reports emphasize that water is a significant factor leading to rock decay; water's role during the weathering process has been inferred to occur in cyclical steps: 1) seepage of meteoric water; 2) dissemination of highly oxidizing meteoric water; 3) triggering of oxidation and dissolution of minerals; 4) water evaporation; and 5) partial migration of the elements contained in the aqueous solution and consequent deposition of minerals in the joints (Bozzano et al. 2006).

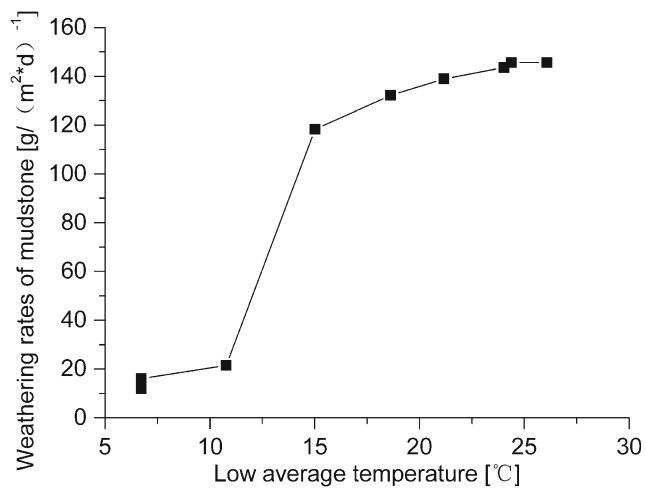
Mudstone weathers and disintegrates easily under sun exposure and rainfall, and this effect is enhanced in summer. Heating and cooling, wetting and drying, and freezing and thawing are known to be the main processes responsible for the physical disintegration of rocks under natural conditions (Erguler and Shakoor 2009). Therefore, much research attention has been focused on the properties of mudstone under dry-wet cycles (Cantón et al. 2001; Erguler and Shakoor 2009; Guo et al. 2012; Yang et al. 2014; Higuchi et al. 2014; Zhang et al. 2015; Qi et al. 2015). When mudstone is exposed to dry-wet cycles, its cementing agents often break down, resulting in mechanical erosion (Imumorin and Azam 2011)

and causing disintegration into gravel and sand-sized particles (Doostmohammadi et al. 2009). Cantón et al. (2001) found that the number of dry-wet cycles had the strongest influence on weathering. Guo et al. (2012) studied the effect of the alternation of heat and water on the slaking phenomenon of redbeds and concluded that the disintegration of mudstone is the result of the comprehensive action of wetting, heating and loading. Yang et al. (2014) investigated the micro-fracture mechanism of mudstone after wet-dry cycles. Qi et al. (2015) concluded that the main mechanisms of slaking of red strata mudstone were water-absorption, dehydration shrinkage during drying and mineral dissolution. Although research under controlled conditions offer insight, there is still a large difference relative to natural conditions, which is limited by the test method. Most of the previous investigators have involved laboratory tests (Cantón et al. 2001; Erguler and Shakoor 2009; Yang et al., 2014; Qi et al., 2015; Zhang et al. 2016), outdoor tests (Guo et al. 2012; Gautam and Shakoor 2013) and in situ monitoring (Yang, et al. 2006; Cantón et al. 2001) to assess the disintegration of mudstone. Among these methods, the in situ monitoring test is closest to natural conditions. However, when restricted by test sites and testing conditions, additional research is needed to evaluate the slaking behaviour of mudstone under laboratory conditions. Therefore, the customized model test device and different dry-wet cycle test conditions are described in this article and were used to study the trends of vertical displacement, crack width and wetted area in mudstone. The crack development law after dry-wet cycles is analysed from three aspects, namely, the temperature-induced stress, load effects and fluid effects, to characterize the ground collapse mechanism in alternating layers of sandstone and mudstone.

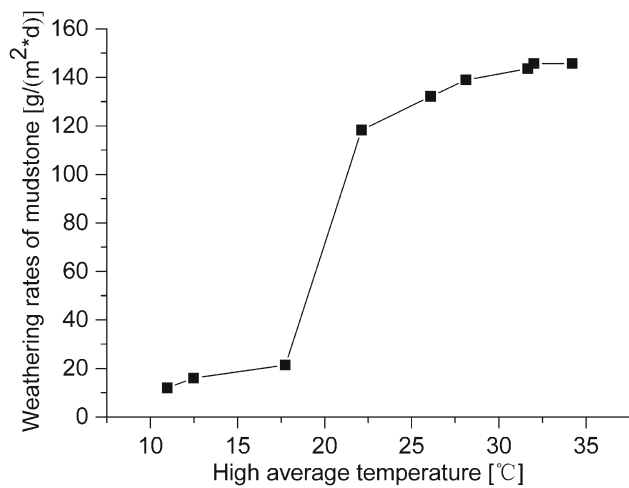
Experimental methodology

The main exogenic effects of mudstone weathering are temperature and rainfall (Yang et al. 2006). Based on the literature (Yang et al. 2006), Fig. 1 shows the relation between the temperature and weathering rates of mudstone based on the monitoring results under the natural state outside (including rainfall) for one year. As shown in Fig. 1, the weathering rates increase with increasing temperature. Therefore, the dry-wet cycle test is designed based on the water-weakening effect and rapid weathering under high temperature.

The experimental materials selected are typical mudstones from the mudstone layers of the Suining group (J_3s) located in the Jinfeng district of Chongqing, south-western China ($N29^{\circ}30'46.05''$, $E106^{\circ}18'55.03''$). Bedrock comprises alternating sandstone and mudstone layers and covers most parts of the Jinfeng area. The climate of the sampled region is subtropical, with an annual average temperature of $18.4^{\circ}C$ and rainfall of 1151.5 mm. Sampling site is shown in Fig. 2.



a Relationship between low average temperature and weathering rates



b Relationship between high average temperature and weathering rates

Fig. 1 Relationship between temperature and weathering rates

Samples were packed with plastic wrap before being sent back to the lab to maintain its original state to the largest degree possible. Samples were cut into a cuboid measuring $300 \times 180 \times 180$ mm with an electric saw and drilled through with an electric drill by a 20 mm diameter borehole that was the channel of inlet water and drainage from the centre of the rectangle top surface to the bottom surface of the sample. The mineral components of the sample are shown in Table 1 (Zhang 2008).

The customized testing device, as shown in Fig. 3, includes a lever-loading device, a container, a thermostat-controlled heating plate and a drainage device. The lever-loading device provides a constant load for the sample by which the load can be increased or decreased by changing weights. The sample is placed in the container, and lateral restraint for the sample is provided by tightening the nuts of the activity steel plate.

Constraint conditions and the loading range are indicated in Fig. 4. The heating plate is a series connection with a temperature controller, a thermocouple and a relay, which can control the temperature and maintain a constant temperature. When used to heat the mudstone, the constant-temperature device can accelerate the test process and enable study of the mudstone weathering process to a certain extent in the laboratory.

The dry-wet cycle test is conducted using the heating plate to heat the sample and by maintaining a water supply and drainage using the top-down drilling hole. The test process is as follows: heating for 24 h at 70°C → water exposure for 8 h → heating for 24 h at 70°C → water exposure for 8 h. The period of each cycle is 32 h. We maintain a constant load, applying a 120 kPa distributed load on the rectangular surface with the scope being 100×100 mm centred around the borehole. The water flow is 82.8 kg/h.

Four dial indicators are used to measure the vertical displacement, as shown in Fig. 5. The A and B sides are unconstrained sides, and the left and right sides are constrained sides. The crack width and the infiltration area are both observed from the unconstrained sides and measured by the crack width observation instrument (minimum scale is 0.05 mm and measuring range is 4 mm) and coordinate paper, respectively.

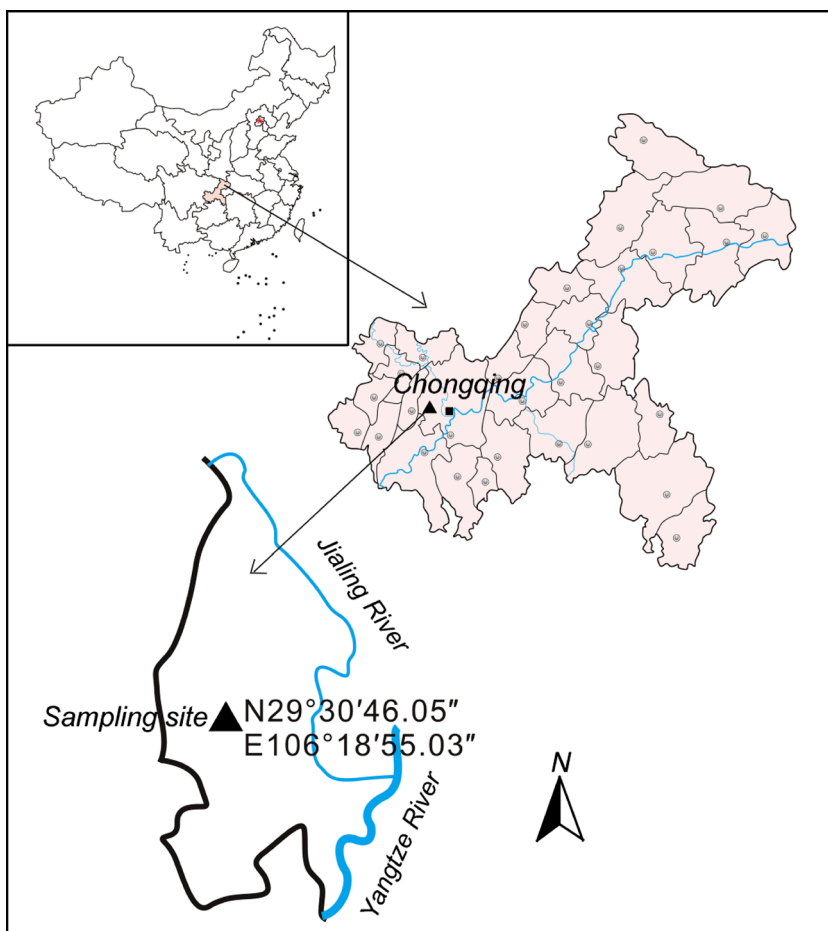
Experimental results

Three dry-wet cycles were conducted. In the first dry-wet cycle, there were cracks on the surface of the sample after heating for 24 h, but these cracks were difficult to detect. With an increase in water exposure time, the crack width continuously expanded, and the surface was not infiltrated. In the second dry-wet cycle, the crack widths decreased after heating for 24 h, and water infiltrated one side of the surface of the sample after water exposure for 1 h and the other side after water exposure for 6 h. The crack width increased, and then became stable. In the third dry-wet cycle, the cracks widths decreased after heating for 24 h, and water infiltrated immediately after water exposure, with the infiltration area constantly expanding. The infiltration speed was faster than that of the second dry-wet cycle; the crack width first increased, then decreased.

Vertical displacement

The change of the vertical displacement of three dry-wet cycles with water exposure time is shown in Table 2. The vertical displacement was measured by dial indicators when the supply water was initiated. The vertical displacement was upwards, indicating that the mudstone swelled when exposed to water. During the initial 3 h of the first dry-wet cycle, the vertical displacement did not change; it subsequently increased and then stabilized. The displacement during the

Fig. 2 Sampling site



second and third dry-wet cycle increased monotonically after water exposure, then became stable.

Figure 6 shows the change of the average displacement of each measuring point of each dry-wet cycle with water exposure time. The displacement increased to a stable value after each dry-wet cycle. The cumulative displacement of the third dry-wet cycle was 2.35 mm. Continual crack expansion resulted in the water continuously contacting the sample. The swelling after water absorption caused the vertical displacement to increase continually.

Crack width

There was no crack on the surface of the undisturbed sample. After heating for 24 h, a slight crack appeared on the surface,

which continually extended and expanded after water exposure. A fixed position was chosen to observe the crack width. Segments of the experiment photos of the crack development and infiltration area are shown in Fig. 7. Figure 8 shows the crack width behaviour with increasing water exposure time.

Figures 7 and 8 show that with increasing water exposure time, the crack width during the first and second dry-wet cycles increased and then stabilized after water exposure for a certain time. The crack width of the first dry-wet cycle was largely stable after water exposure for 5 h, and the crack width of the second dry-wet cycle changed slightly after water exposure for 2 h. The crack width of the third dry-wet cycle first increased and then decreased after water exposure for 1–2 h because the water infiltrated through cracks into the surface to make the sample swell; subsequently, the crack width was reduced. In addition, the crack width of each dry-wet cycle

Table 1 Content of clay mineral and non-clay mineral of mudstone (Zhang 2008)

Position	Type and content of mineral (%)				
	Quartz	Potassium feldspar	Anorthose	Hematite	Clay mineral
Suining group	25.9	0.9	12.9	3.9	56.4



a Drying



b Wetting

Fig. 3 Photos of the whole test device

after heating was smaller than that of the last dry-wet cycle, which was due to the thermal expansion that caused the sample to swell. There were no cracks on the surface of the original mudstone, but cracks were generated when the moisture inside the mudstone slowly evaporated after heating.

Wetted area

Selected pictures of the wetted area are shown in Fig. 7. Figure 9 shows the change of the wetted area with water exposure time. No water infiltrated the surface of the sample in the first dry-wet cycle. Water infiltrated slowly to the B side in the second dry-wet cycle. With increasing water exposure time, the wetted area increased, suggesting that the crack from the borehole to the surface of this side connected and that the permeability coefficient increased. There was no water

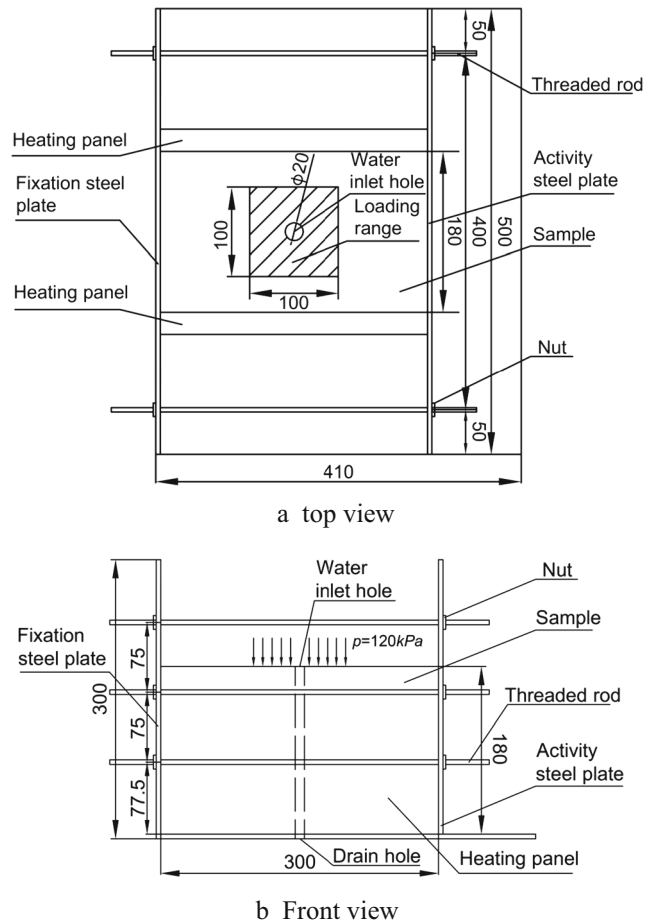


Fig. 4 Container used in experiments (unit: mm)

infiltration on the A side until water exposure had been conducted for 5 h, after which the wetted area increased. After heating during the third dry-wet cycle, the water wetting on the surface of the previous dry-wet cycle evaporated, and water immediately infiltrated after water exposure. The infiltration rate was significantly faster than the second dry-wet cycle. The internal cracks expanded with successive dry-wet cycles and connected continuously between one crack and

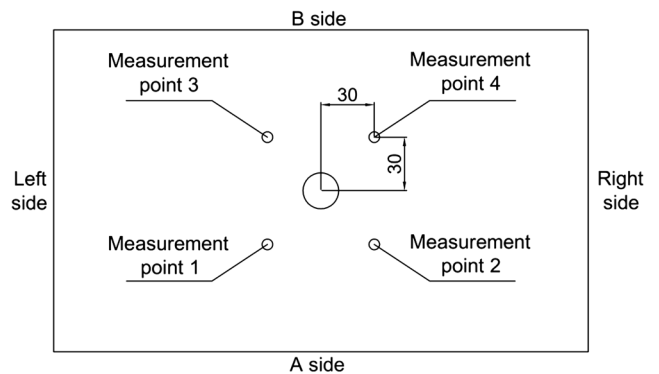


Fig. 5 Displacement measurement points (unit: mm)

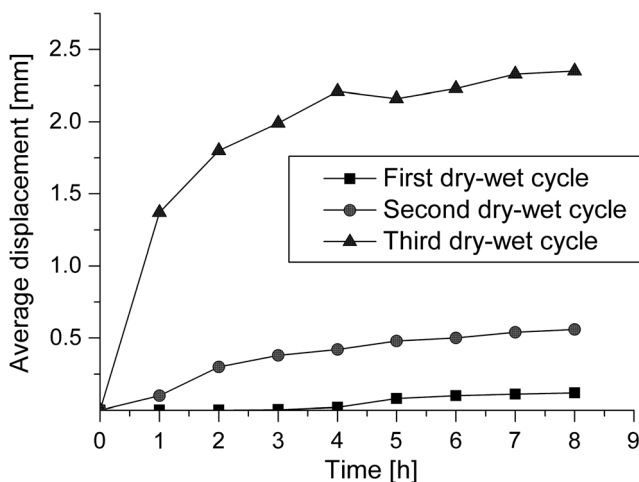
Table 2 Vertical displacement with watering exposure time

Time/h		1	2	3	4	5	6	7	8
Displacement/mm									
Measurement point	Cycle number								
1	First	0	0	0	0	0.08	0.09	0.10	0.12
2		0	0	0	0.03	0.08	0.10	0.11	0.12
3		0	0	0	0.02	0.07	0.08	0.09	0.10
4		0	0	0	0.02	0.1	0.12	0.13	0.13
Average		0	0	0	0.02	0.08	0.09	0.10	0.12
1	Second	0.02	0.08	0.18	0.24	0.27	0.32	0.35	0.39
2		0.26	0.42	0.47	0.47	0.53	0.53	0.60	0.60
3		0.03	0.29	0.38	0.44	0.58	0.58	0.62	0.66
4		0.32	0.43	0.48	0.51	0.56	0.56	0.58	0.58
Average		0.16	0.30	0.38	0.42	0.48	0.50	0.54	0.56
1	Third	1.49	2.01	2.26	2.43	2.43	2.43	2.43	2.43
2		1.40	1.88	2.03	2.21	2.28	2.40	2.57	2.57
3		0.86	1.09	1.16	1.28	1.35	1.41	1.46	1.48
4		1.72	2.22	2.51	2.93	2.58	2.69	2.86	2.92
Average		1.37	1.80	1.99	2.21	2.15	2.23	2.33	2.35

another crack, while the permeability coefficient and seepage speed both increased.

Discussion

The initiation and propagation of macro cracks in rocks results from the combined action of temperature-induced stress, load effects and fluid effects. Therefore, studying the mechanism of these factors is the basis for observing the changes of macro cracks in mudstone. This study focuses primarily on analysing the effect of these three fac-

**Fig. 6** Vertical average displacement with watering exposure time

tors on mudstone from the perspective of mechanical analysis as follows.

Temperature-induced stress

When rock expansion caused by a change of temperature is constrained, stress is produced. This stress constitutes thermal stress generated when thermal expansion is constrained without the effect of external force.

The thermal expansion coefficient of mudstone is $\alpha = 9 \times 10^{-6} / ^\circ\text{C}$ (Tang et al. 2006), the Young's modulus $E = 2 \times 10^9$ Pa and Poisson's ratio $\mu = 0.3$. αE in each direction is constant. The temperature distribution and the temperature-induced stress distribution are shown in Fig. 10. The temperature-induced stress is (Li 2004)

$$\sigma_x = \frac{\alpha E}{1-\mu} \left[-t(y) + \frac{1}{c-0.01} \int_{0.01}^c t(y) dy \right] \quad (1)$$

The calculation method of σ_z is the same as σ_x , whose difference from σ_x is without borehole. This assumes that the temperature distribution along the y axis in Fig. 10 is (Li 2004)

$$t(y) = t_0 \left[1 - \frac{y^2}{a} \right] \quad (2)$$

The uniform temperature load of 70°C is applied on the surface of mudstone, and temperature is 24°C (room

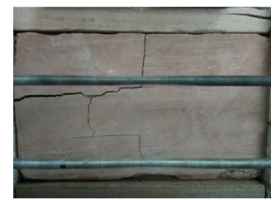
Fig. 7 Segment of photos of crack width and wetted area



Heating 24h



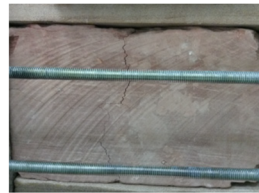
Watering exposure 1h
A side



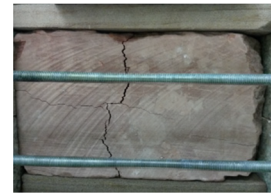
Watering exposure 8h



Heating 24h

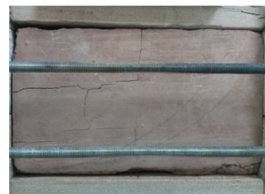


Watering exposure 1h
B side



Watering exposure 8h

a The first dry-wet cycle



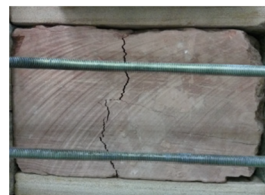
Heating 24h



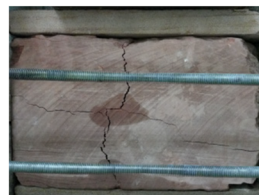
Watering exposure 1h
A side



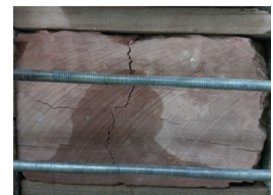
Watering exposure 8h



Heating 24h



Watering exposure 1h
B side

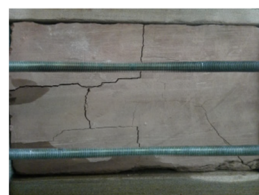


Watering exposure 8h

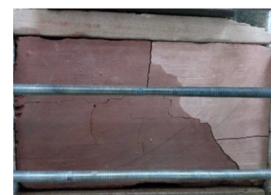
b The second dry-wet cycle



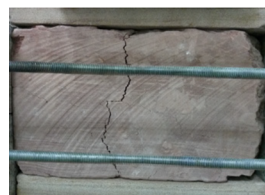
Heating 24h



Watering exposure 1h
A side



Watering exposure 8h



Heating 24h



Watering exposure 1h
B side



Watering exposure 8h

c The third dry-wet cycle

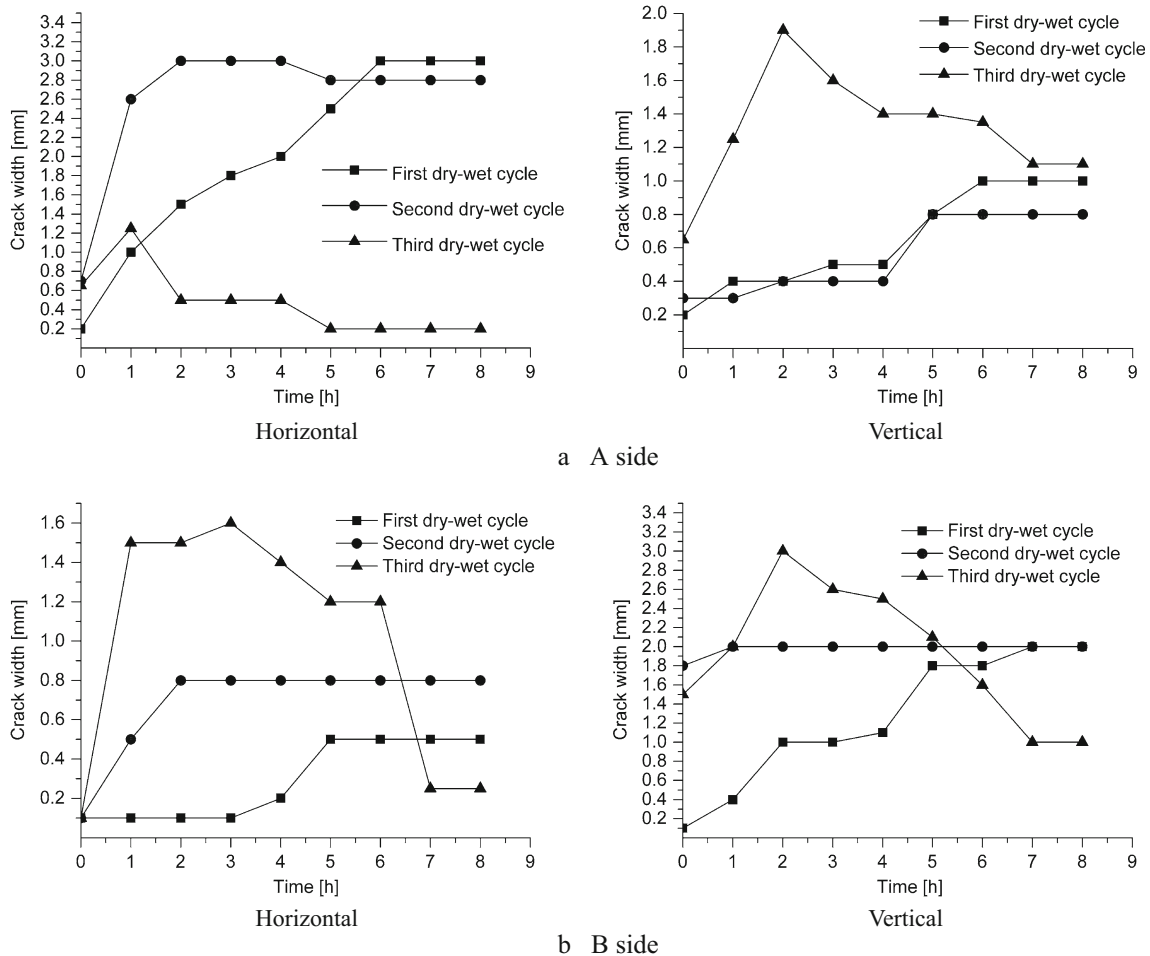


Fig. 8 Change of crack width with watering exposure time

temperature) inside the borehole, so when $y = 0.01$, $t(y) = 24$ and $y = 0.09$, $t(y) = 70$. Substituting these boundary conditions into Eq. (2), it obtains $t_0 = 23.44$ and $a = -0.0041$. Substituting t_0 and a into Eq. (2), the temperature distribution along the y axis is obtained as follows.

$$t(y) = 23.44(1 + 243.9y^2) \tag{3}$$

Substituting Eq. (3) into Eq. (1), we obtain

$$\sigma_x = \frac{\alpha E}{1-\mu} (-5717.02y^2 + 17.34) \tag{4}$$

Inserting parameters into Eq. (4), the temperature-induced stress distribution along the y direction, as shown in Fig. 10b, is obtained. Due to the high temperature on the outer boundary and the low temperature around the borehole, the outer boundary undergoes compressive stress with a maximum value of 0.43 MPa. The borehole undergoes tensile stress with a

maximum value of 0.74 MPa. The turning point between the tensile stress and the compression stress is located at $y = 0.055$ m. When $y \in (0, 0.055)$, if the tensile stress is greater than the tensile strength, cracks are initiated. When $y \in (0.055, 0.09)$, cracks on the surface will not be produced by the effect of thermal stress and will actually assist in crack closure, which explains the surface crack decrease after heating in each dry-wet cycle.

Load effects

The stress distribution within homogeneous continuous rock masses under load effects can be solved by the finite element method. The finite element software ANSYS is applied to calculate the stress distribution under the action of uniform loading. The computing model is shown in Fig. 11, whose coordinate system matches that of Fig. 10. Mudstone is simulated by the 8-node SOLID45 element. The A surface, B

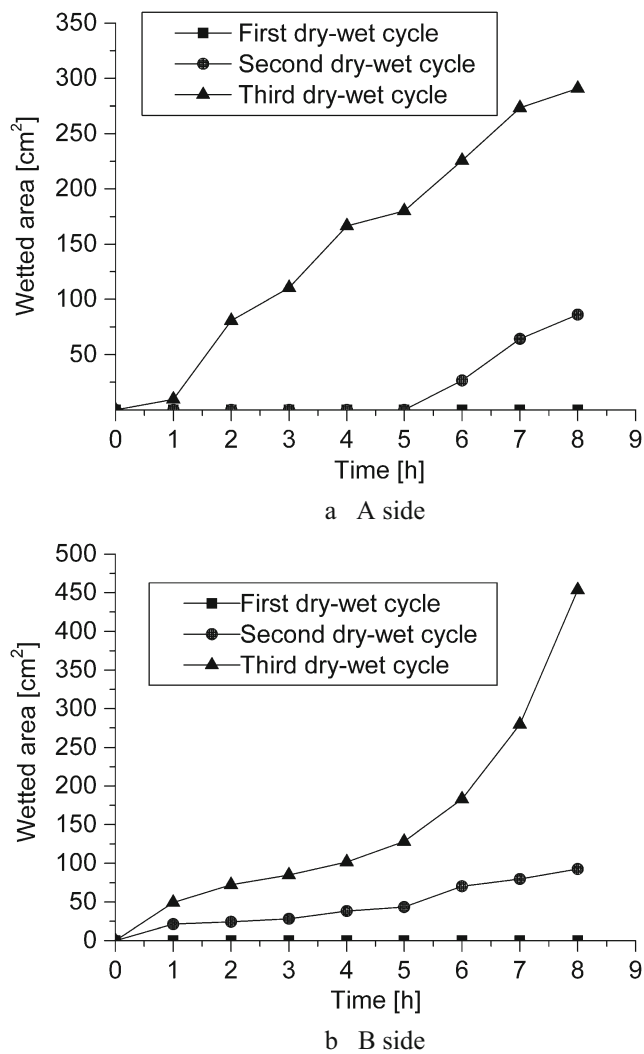


Fig. 9 Change of wetted area with watering exposure time

surface and upper surface of the computing model are free boundary. The x direction constraint is imposed on the right and left surface, and full constraints are imposed on the bottom surface. The uniform distribution load of 120 kPa is applied on the top surface. Drucker-Prager model is applied to the computing model, and material parameters are shown in Table 3. Figure 12 shows the x -component of stress, y -component of stress and z -component of stress, respectively.

From Fig. 12a, along the x direction on the top surface of the sample, when $x < 0.1$ m (within the loading range), compressive stress occurs with a maximum value of 26.98 kPa; when $x > 0.1$ m (beyond the loading range), tensile stress occurs with a maximum value of 62.69 kPa. Thus, it is not easy to generate cracks around the borehole (within the loading range). Cracks will be produced beyond the loading range when the load is greater than the tensile strength of the sample

and the extending direction of cracks is perpendicular to the loading direction.

From Fig. 12b, compressive stress occurs along the y direction on the top surface of the sample with a maximum of 18.09 kPa. Therefore, cracks will not be generated within the loading range.

Each starting location of the z direction is shown in Fig. 12c. Curve 1 is the inner surface of the borehole on the constrained side, and it undergoes tensile stress with a maximum value of 42.16 kPa. Curve 3 is the inner surface of the borehole on the unconstrained side and undergoes compressive stress with a maximum value of 6.37 kPa. Curve 2 is the unconstrained surface, and it undergoes compressive stress with a maximum value of 0.035 kPa. Thus, cracks will not be generated on the A and B surface, but cracks will be produced inside the borehole and the extending direction of cracks is perpendicular to the loading direction.

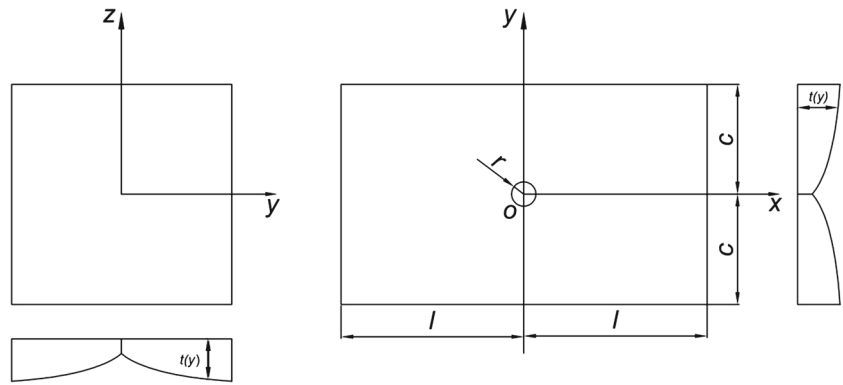
Therefore, load effects promote the formation of cracks on the unconstrained surface but inhibit the formation of cracks on the constrained surface. When the overlying load is small, the effect of the sample is limited.

Fluid effects

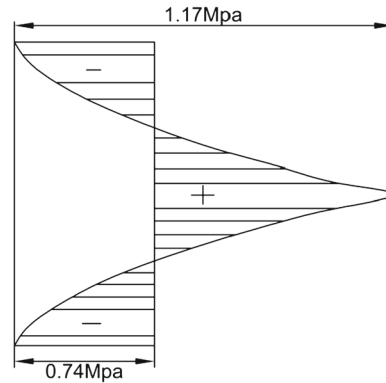
Micro cracks and micro holes existed before macroscopic cracks appeared in the sample. The structure's mesoscopic damage elements (such as micro cracks and micro holes) constantly initiate, join and extend until connection, which causes the performance of mudstone to deteriorate under the effect of a load or the environment (e.g. temperature change, fluid effects or corrosion). This evolution process constitutes the damage mechanism. The fracture occurs in the later stages after damage in the material and represents the limit state in which the stress capacity of the material is completely lost. Visible cracks are produced with the extension of the structure's mesoscopic damage elements after heating, which provides a channel for the water to infiltrate, causing the contact area between water and mudstone to continually increase. Under the action of hydraulic fracturing and the water-weakening effect, cracks connect with each other and the crack width increases, eventually reaching the limit state and failure.

Kang (1994) obtained a rock damage variable evolution equation associated with the expansion under the influence of water using the theory of the damage mechanics that can well describe the rock damage characteristics under the influence of water. In a previous study, Guo et al. (2012) analysed crack generation and fracture mechanisms in mudstone from the microscopic angle. The crack propagation conditions are explained primarily through hydraulic fracturing as follows.

Fig. 10 Temperature distribution and stress along the y direction



a Temperature distribution



b Temperature-induced stress distribution

The stress of a single crack is shown in Fig. 13. σ_1 and σ_3 are the maximum and minimum principal stress, respectively; σ_α and τ_α are the normal stress and shear stress of the crack, respectively; p_{hs} and p_{hd} are the hydrostatic pressure and hydrodynamic pressure, respectively; a and b are the length and the width of the crack, respectively, and α is the angle between the extension direction of the crack and the maximum principal stress. Zhu and Hu (2000) deduced the initial cracking strength formula by considering the fissure

water pressure of rocks but did not consider the effect of dynamic water pressure. Therefore, this article incorporates dynamic water pressure into the formula.

Based on the literature (Wu and Zhang 1995), the normal and shear stresses of the crack are

$$\sigma_\alpha = \frac{\sigma_1 + \sigma_3}{2} - \frac{\sigma_1 - \sigma_3}{2} \cos 2\alpha \tag{5}$$

$$\tau_\alpha = \frac{\sigma_1 - \sigma_3}{2} \sin 2\alpha \tag{6}$$

When seepage pressure p_{hs} and p_{hd} exist in the crack, assuming water cannot infiltrate the rock, the stresses containing seepage water pressure on the surface of the crack are

$$\sigma_\alpha^w = \frac{\sigma_1 + \sigma_3}{2} - \frac{\sigma_1 - \sigma_3}{2} \cos 2\alpha - p_{hs} \tag{7}$$

$$\tau_\alpha^w = \frac{\sigma_1 - \sigma_3}{2} \sin 2\alpha - p_{hd} \tag{8}$$

Beginning from the closed crack and by setting c_i and f_i equal to the cohesion and the friction coefficient on the surface of the crack, respectively, the friction resistance on the surface of the crack is

$$F = c_i + f_i \sigma_\alpha^w \tag{9}$$

Therefore, the resultant force parallel to the plane of the crack is

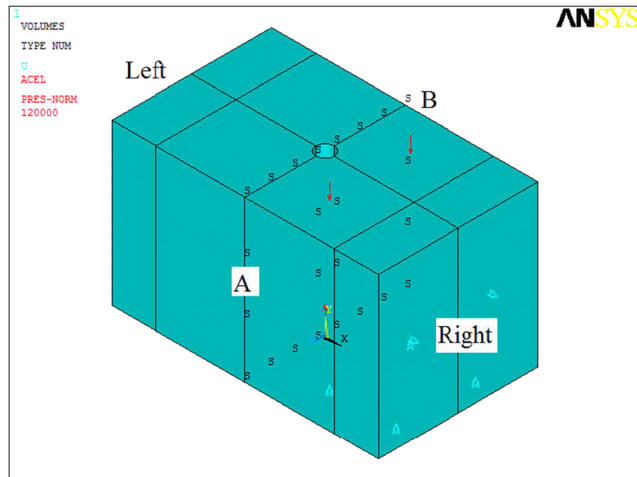
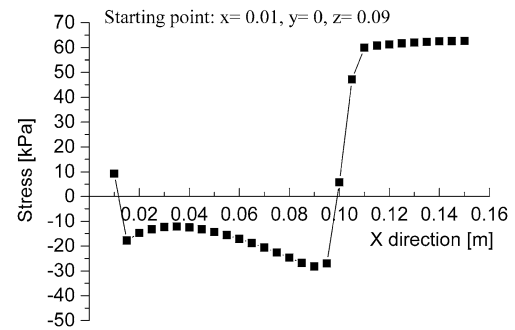
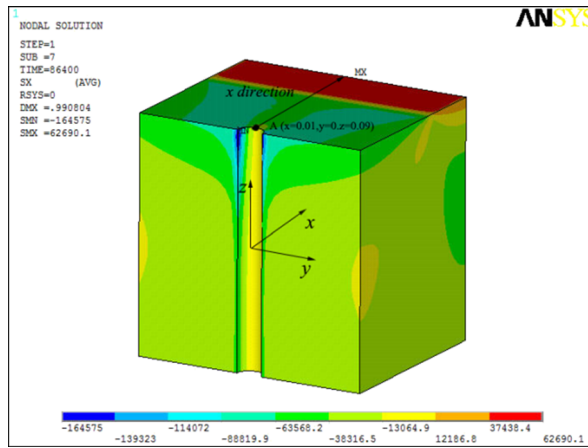


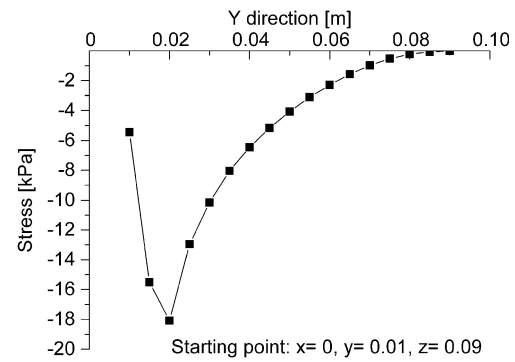
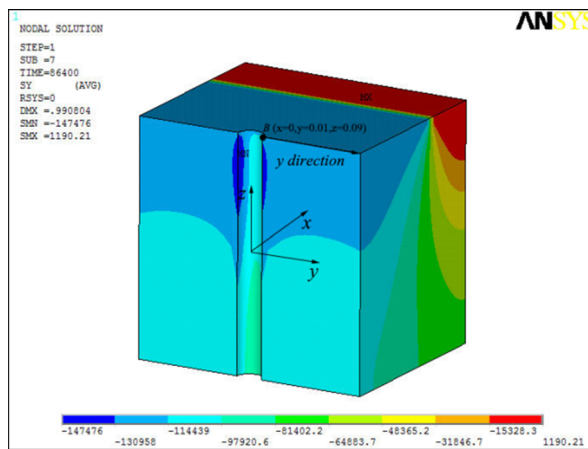
Fig. 11 Computing model of load effects

Table 3 The material parameters

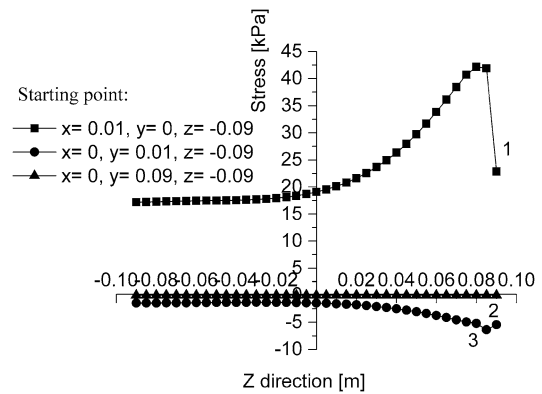
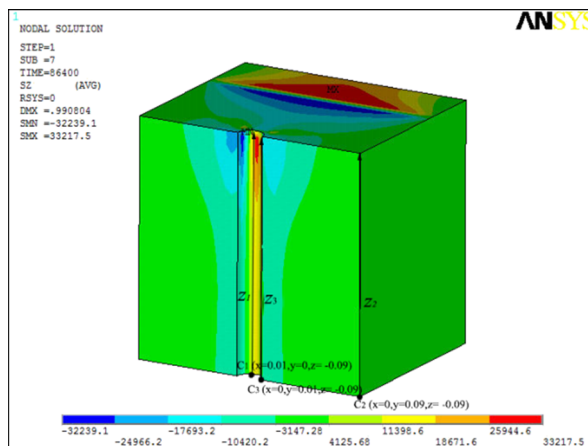
	Young's modulus (Pa)	Poisson's ratio	Unit weights (kN/m ³)	Cohesion (Pa)	Internal friction angle (°)
Mudstone	2e9	0.3	25.4	5.7e5	32



a x-Component of stress



b y-Component of stress



c z-Component of stress

Fig. 12 Change of stress along the x, y, z direction

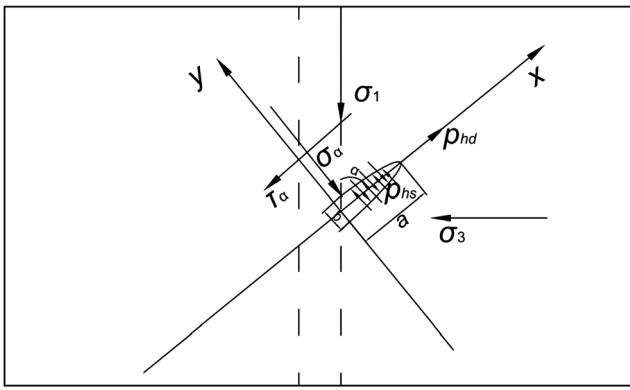


Fig. 13 Stress of a single crack

$$\tau = \tau_{\alpha}^w - F \tag{10}$$

The seepage pressure is (Wu and Zhang 1995)

$$p_{hs} = \gamma H \tag{11}$$

$$p_{hd} = \gamma J_f \exp[\mu \gamma H - \mu (\sigma_1 \sin^2 \alpha + \sigma_3 \cos^2 \alpha)] \tag{12}$$

where γ is the unit weight of water; H is the water head of the crack; J_f is the hydraulic gradient; and μ is the undetermined coefficient.

According to the theory of fracture mechanics, the tip stress intensity factor of the open type crack is

$$K_I = -\sigma_{\alpha} \sqrt{\pi a} \tag{13}$$

$$K_{II} = \tau_{\alpha} \sqrt{\pi a} \tag{14}$$

Substituting Eqs. (7) and (11) into Eq. (13) and substituting Eqs. (8), (9), (10) and (12) into Eq. (14) gives the following:

$$K_I = -\left(\frac{\sigma_1 + \sigma_3}{2} - \frac{\sigma_1 - \sigma_3}{2} \cos 2\alpha - p_{hs}\right) \sqrt{\pi a} \tag{15}$$

$$K_{II} = \left[(\sin 2\alpha + f_i \cos 2\alpha - f_i) \frac{\sigma_1}{2} - (\sin 2\alpha + f_i \cos 2\alpha + f_i) \frac{\sigma_3}{2} + p_{hs} f_i - c_i - p_{hd} \right] \sqrt{\pi a} \tag{16}$$

According to the maximum circumferential stress criterion, the relation of the stress intensity factor of I- and II-type cracks is

$$K_I \sin \theta + K_{II} (3 \cos \theta - 1) = 0 \tag{17}$$

where θ is the crack propagation angle.

Substituting Eqs. (15) and (16) into Eq. (17), we can determine the crack propagation angle $\theta = \theta_0$. Substituting it into the tip crack equation in polar coordinates, we obtain

$$\begin{aligned} (\sigma_{\theta})_{\max} &= (\sigma_{\theta})_{\theta=\theta_0} \\ &= \frac{1}{2\sqrt{2\pi r}} \cos \frac{\theta_0}{2} [K_I (1 + \cos \theta_0) - 3K_{II} \sin \theta_0]. \end{aligned} \tag{18}$$

The threshold cracking condition is thus determined.

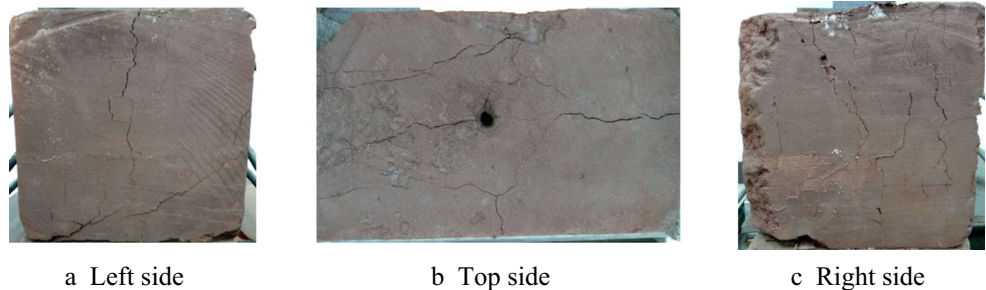
Above all, the temperature-induced stress and the load effects cause the inner portion of the sample to undergo tensile

stress and the surface to undergo compressive stress. When stress arises from temperature-induced stress and the overlying load is greater than the tensile strength of the mudstone, internal cracks initiate and provide channels for water. The fracturing effect of water then causes these cracks to extend to the outer surface of the sample. The sample fractures into several pieces under repeated dry-wet cycles, as shown in Fig. 14.

Conclusion

The crack development mechanism of mudstone is explored over multiple dry-wet cycles. Tiny cracks appear on the surface of the sample after heating. With increasing water exposure time, the crack widths expand. However, after the water wets the surface of the sample, the crack widths decrease. With successive dry-wet cycles, the wetting speed is

Fig. 14 Cracks on the surface



a Left side

b Top side

c Right side

progressively faster, indicating that the number and size of the internal cracks in the sample gradually increase. The sample fractures when a crack propagates through it.

Temperature-induced stress, load effects and fluid effects are analysed to explore the crack development mechanism. The temperature-induced stress and the load effects cause the inner portion of the sample to undergo tensile stress and the surface to undergo compressive stress. When the stress produced by temperature and the overlying load is greater than the tensile strength of the mudstone, internal cracks initiate, providing channels for the action of water and causing the contact area between water and mudstone to constantly increase. Under the action of hydraulic fracturing and the water-weakening effect, cracks connect, and the crack widths increase, eventually inducing failure.

A customized model test container and novel test method is applied to provide a reference for the degradation of other rock masses. The model test device and the test method of the dry-wet cycles are different from previous similar tests and give full consideration to the combined action of temperature-induced stress, load and fluid effects. The test conditions are closer to those of actual situations. The relevant test methods and test results can provide a reference for the degradation of other rock masses.

Acknowledgements The authors gratefully acknowledge the financial support from the Chongqing Research Program of Basic Research and Frontier Technology (No. cstc2015jcyjBX0073) and the science and technology project of Land Resources and Real Estate Management Bureau of Chongqing Government (No. CQGT-KJ-2014052).

References

- Al-homoud AS, Kuoury H, Al-Omari YA (1996) Mineralogical and engineering properties of problematic expansive clayey beds causing landslides. *Bull Eng Geol Environ* 54:13–31. doi:10.1007/BF02600651
- Amould M (2006) Discontinuity networks in mudstones: a geological approach—implications for radioactive wastes isolation in deep geological formations in Belgium, France, Switzerland. *Bull Eng Geol Environ* 65(4):413–422. doi:10.1007/s10064-006-0060-3
- Ashby MF, Raj R, Gifkins C (1970) Diffusion controlled sliding at a serrated grain boundary. *Scr Metall* 4(9):737–741. doi:10.1016/0036-9748(70)90216-4
- Bozzano F, Gaeta M, Marcoccia S (2006) Weathering of valle ricca stiff and jointed clay. *Eng Geol* 84(3–4):161–182. doi:10.1016/j.enggeo.2005.11.010
- Cantón Y, Solé-Benet A, Queralt I, Pini R (2001) Weathering of a gypsum-calcareous mudstone under semi-arid environment at Tabernas, SE Spain: laboratory and field based experimental approaches. *Catena* 44(2):111–132. doi:10.1016/S0341-8162(00)00153-3
- Doostmohammadi R, Moosavi M, Mutschler TH, Osan C (2009) Influence of cyclic wetting and drying on swelling behavior of mudstone in south west of Iran. *Environ Geol* 58:999–1009. doi:10.1007/s00254-008-1579-3
- Eeckhout EMV (1976) The mechanisms of strength reduction due to moisture in coal mine shales. *Int J Rock Mech min Sci Geomech Abstr* 13(2):61–67. doi:10.1016/0148-9062(76)90705-1
- Einstein HH (1996) Tunnelling in difficult ground—swelling behaviour and identification of swelling rocks. *Rock Mech Rock Eng* 29(3):113–124. doi:10.1007/BF01032649
- Erguler ZA, Shakoor A (2009) Relative contribution of various climatic processes in disintegration of clay-bearing rocks. *Eng Geol* 108(1–2):36–42. doi:10.1016/j.enggeo.2009.06.002
- Erguler ZA, Ulusay R (2009) Water-induced variations in mechanical properties of clay-bearing rocks. *Int J Rock Mech min* 46(2):355–370. doi:10.1016/j.ijrmmms.2008.07.002
- Gamble JC (1971) Durability-plasticity classification of shales and other argillaceous rock. Dissertation, University of Illinois
- Goodman RE (1989) Introduction to rock mechanics, 2nd edn. Wiley, New York
- Gautam TP, Shakoor A (2013) Slaking behavior of clay-bearing rocks during a one-year exposure to natural climatic conditions. *Eng Geol* 166:17–25. doi:10.1016/j.enggeo.2013.08.003
- Guo YC, Xie Q, Wen JQ (2012) Effect of the alternation of heat and water on the slaking phenomenon of redbeds. *Hydrogeol Eng Geol* 39(5):69–73 (in Chinese)
- Higuchi K, Chigira M, Lee D-H, Wu J-H (2014) Rapid weathering and erosion of mudstone induced by saltwater migration near a slope surface. *J Hydrol Eng* 20(6):C6014004. doi:10.1061/(ASCE)HE.1943-5584.0001105
- Imumorin P, Azam S (2011) Effect of precipitation on the geological development of badlands in arid regions. *Bull Eng Geol Environ* 70(2):223–229. doi:10.1007/s10064-010-0300-4
- Jiang Q, Cui J, Feng XT, Jiang Y (2014) Application of computerized tomographic scanning to the study of water-induced weakening of mudstone. *Bull Eng Geol Environ* 73(4):1293–1301. doi:10.1007/s10064-014-0597-5
- Kang HP (1994) Rock damage caused by water. *Hydrogeol Eng Geol* 3:39–41 (in Chinese)
- Lee D-H, Chen PY, Wu J-H et al (2013) Method of mitigating the surface erosion of a high-gradient mudstone slope in southwest Taiwan. *Bull Eng Geol Environ* 72(3):533–545. doi:10.1007/s10064-013-0518-z
- Lashkaripour GR (2002) Predicting mechanical properties of mudrock from index parameters. *Bull Eng Geol Environ* 61(1):73–77. doi:10.1007/s10064100116
- Lashkaripour GR, Boomeri M (2002) The role of mineralogy on durability of weak rocks. *J Appl Sci* 2(6):698–701. doi:10.3923/jas.2002.698.701
- Li WT (2004) The theory analysis and application of thermal stress. China Electric Power Press, Beijing (in Chinese)
- Lu Y, Wang L, Sun X, Wang J (2016) Experimental study of the influence of water and temperature on the mechanical behavior of mudstone and sandstone. *Bull Eng Geol Environ*:1–16. doi:10.1007/s10064-016-0851-0
- Molinda GM, Oyler DC, Gurgleni H (2006) Identifying moisture sensitive roof rocks in coal mines. Proceedings of 25th International Conference on Ground Control in Mining. West Virginia University, Morgantown, pp 57–64
- Ojo O, Brook N (1990) The effect of moisture on some mechanical properties of rock. *Min Sci Technol* 10(2):145–156. doi:10.1016/0167-9031(90)90158-O
- Phienweij N (1987) Ground response and support performance in a sheared shale, Stillwater Tunnel. Dissertation, University of Illinois
- Poulsen BA, Shen B, Williams DJ, Huddleston-Holmes C, Erarslan N, Qin J (2014) Strength reduction on saturation of coal and coal measures rocks with implications for coal pillar strength. *Int J Rock Mech min* 71:41–52. doi:10.1016/j.ijrmmms.2014.06.012
- Pejon OJ, Zuquette LV (2002) Analysis of cyclic swelling of mudrocks. *Eng Geol* 67(1–2):97–108. doi:10.1016/S0013-7952(02)00147-3

- Qi J, Sui W, Liu Y, Zhang D (2015) Slaking process and mechanisms under static wetting and drying cycles slaking tests in a red strata mudstone. *Geotech Geol Eng* 33(4):959–972. doi:[10.1007/s10706-015-9878-4](https://doi.org/10.1007/s10706-015-9878-4)
- Silva MRD, Schroeder C, Verbrugge J-C (2008) Unsaturated rock mechanics applied to a low-porosity shale. *Eng Geol* 97(1–2):42–52. doi:[10.1016/j.enggeo.2007.12.003](https://doi.org/10.1016/j.enggeo.2007.12.003)
- Seedsman RW (1993) Characterizing clay shales. In: Hudson JA (ed) comprehensive rock engineering, vol. 3. Pergamon Press, Oxford, pp 151–164
- Tang SB, Tang CA, Zhu WC et al (2006) Numerical investigation on rock failures process induced by thermal stress. *Chin J Rock Mech Eng* 25(10):2071–2078 (in Chinese)
- Wu YQ, Zhang ZY (1995) An introduction to rock mass hydraulics. Southwest jiaotong university press, Chengdu (in Chinese)
- Yoshida N, Nishi M, Kitamura M, Adachi T (1997) Analysis of mudstone deterioration and its effect on tunnel performance. *Int J rock Mech min Sci* 34(3–4): 353. e1–353. e19. doi: [10.1016/S1365-1609\(97\)00289-X](https://doi.org/10.1016/S1365-1609(97)00289-X)
- Yang JL, Wang LG, Li XL, Zhao G (2014) Research on micro-fracture mechanism of mudstone after wet-dry cycles. *Chin J Rock Mech Eng* 33(A02):3606–3612. (in Chinese). doi:[10.13722/j.cnki.jrme.2014.s2.027](https://doi.org/10.13722/j.cnki.jrme.2014.s2.027)
- Yang ZC, Zhang JY, Zhou DP (2006) Study on fast weathering characteristics of red bed mudstone slope. *Chin J Rock Mech Eng* 25(2): 275–283 (in Chinese)
- Zhang H, Adoko AC, Meng Z, Wang H, Jiao Y (2017) Mechanism of the mudstone tunnel failures induced by expansive clay minerals. *Geotech Geol Eng* 35(1):263–275. doi:[10.1007/s10706-016-0102-y](https://doi.org/10.1007/s10706-016-0102-y)
- Zhang SX (2008) Research on relationship between substantial composing and mechanical parameters of mudstone in Chongqing. Dissertation, Chongqing Jiaotong University (in Chinese)
- Zhang D, Chen A, Wang X, Liu G (2015) Quantitative determination of the effect of temperature on mudstone decay during wet-dry cycles: a case study of ‘purple mudstone’ from south-western china. *Geomorphology* 246:1–6. doi:[10.1016/j.geomorph.2015.06.011](https://doi.org/10.1016/j.geomorph.2015.06.011)
- Zhang D, Chen A, Wang X, Yan B, Shi L, Liu G (2016) A quantitative determination of the effect of moisture on purple mudstone decay in southwestern China. *Catena* 139:28–31. doi:[10.1016/j.catena.2015.12.003](https://doi.org/10.1016/j.catena.2015.12.003)
- Zhu ZD, Hu D (2000) The effect of interstitial water pressure on rock mass strength. *Rock Soil Mech* 21(1):64–67 (in Chinese)